scientific reports

Check for updates

OPEN

Removal mechanism of phosphorus in water by calcium hydroxide modified copper tailings

Yuting Li, Yunnen Chen✉, Jiali Xu & Jun Liu

With the development of industry and agriculture, eutrophication caused by increasing amounts of phosphorus in the environment has attracted people's attention. On the other hand, copper tailings (CT) is a kind of solid waste with large quantity, large area, and easy to cause groundwater and soil pollution. CT is also a potential resource because of its large specific surface area. CT is intended to be used as an adsorbent for removal phosphate in water, but trace heavy metals and a small amount of phosphate in CT may bring negative effects. Calcium hydroxide ($Ca(OH)_2$) was used to modify CT (CCT), hoping to fix the heavy metals and phosphate in CT at the same time. It was found that the removal capacity of CCT was significantly higher than that of CT. The process of phosphate removal by CCT involves electrostatic sorption and surface precipitation, and there is a synergistic effect between CT and $Ca(OH)_2$. The phosphate removal rate of CCT-0.4 increased with the increase of pH value under alkaline conditions. The XRD patterns of phosphate sorption by CCT mean that $Ca_3(PO_4)_2$, $Ca_5(PO_4)_3(OH)$ and $AlPO_4$ exist in CCT after phosphate removal, indicating that surface precipitation occurs during the removal process. In summary, the removal mechanism of phosphate by CCT is mainly electrostatic attraction and surface precipitation.

Keywords Phosphorus, Copper tailings, Calcium hydroxide, Electrostatic attraction, Surface precipitation

Although phosphorus is essential for all living things[1,2], excess phosphate in water is a pollutant. With the development of industry and agriculture, more and more phosphate is released into the water[3]. Even low concentration of phosphorus in water lead to eutrophication[4], reduced oxygen levels, and algal blooms[5].

There are various methods for removal phosphorus in water, including biological methods, chemical methods, and sorption, et al.[5]. The reaction conditions of biological phosphorus removal are harsh and easily affected by water temperature and pH[6]. The disadvantages of chemical methods are high cost and large amount of sludge[7–9]. Compared with these, the sorption has the characteristics of economy, high efficiency and no sludge production[2]. The maximum sorption capacity of lanthanum modified biochar can reach 93.92 mg/g[10]. The sorption capacity of Mg-modified biochar made from ground coffee grounds can reach 56 mg/g[11].

On the other hand, China's copper production ranks third in the world, and copper tailings (CT) produce more than 300 million tons per year[12]. At present, the disposal method of CT is mainly open storage[13], which occupies a large amount of land. CT is not only a solid waste, but also a resource. CT has the characteristics of large specific surface area, many pores and uniform surface charge[14,15]. For example, the specific surface area of CT after grinding can reach 613 m^2/kg[16], which is suitable for sorption of copper ions[17] and dyes[18].

In general, CT contains Al, Ca, Si, and Fe elements that have an affinity for phosphate[19]. However, the composition of CT from different sources is different, as shown in Table 1, resulting in differences in their properties and their ability to removal phosphates[20]. If the physicochemical properties of CT do not meet the relevant requirements, it need to be modified[21]. For example, after thermally modification of CT, the phosphate sorption capacity increased from 2.08 to 14.25 mg/g[22]. The phosphate removal rate of heat-modified CT increased from 83.50 to 96.50%[23]. The sorption capacity of lanthanum-modified CT is 9.6 times that of CT[19]. Studies have shown that calcium hydroxide ($Ca(OH)_2$) modified zeolite can improve the phosphorus removal rate[24].

As two relatively expensive modification methods, neither thermal modification nor lanthanum modification mentioned the mechanism of phosphate sorption by modified CT adsorbent. Based on the cost factor, this study was conducted to investigate the feasibility of $Ca(OH)_2$ modified CT to remove phosphate from natural surface water, and explored its mechanism. First, CT was modified with $Ca(OH)_2$ suspensions as adsorbent of

Jiangxi Key Laboratory of Mining & Metallurgy Environmental Pollution Control, Jiangxi University of Science & Technology, No. 156Kejia Ave., Ganzhou 341000, Jiangxi, People's Republic of China. ✉email: cyn70yellow@126.com

Composition	SiO_2	Al_2O_3	Fe_2O_3	CaO	MgO	K_2O	Na_2O	SO_3	Data source
Content (%)	50.37	12.52	9.75	19.02	2.35	2.06	0.93	1.70	Anhui, China[25]
	22.11	4.19	46.31	1.61	1.94			19.92	Xinjiang, China[26]
	36.26	4.50	34.87	2.79	3.89	1.17	0.68	0.70	Yunnan, China[27]

Table 1. The composition and content of CT from different sources.

phosphate in water. Then, the effects of pH value, contact time and reaction temperature and initial phosphorus concentration on phosphate removal by CCT were studied. Finally, the dephosphorization mechanism of CCT was analyzed by means of BET, XRD and FTIR.

Materials and methods

Experimental materials

The CT used in the experiment came from a copper mine in Jiangxi Province, China.

Phosphate stock solutions were prepared with potassium dihydrogen phosphate as raw material. Stock solution diluted with pure water was used as phosphorus containing solution for experiment. The pH of the solution was adjusted with 0.1 mol/L NaOH and HCl. In the phosphate removal experiments, no buffer was used to control the pH between pH 4–9.

The chemical reagents used were all analytically pure except that ammonium molybdate was excellent pure.

A certain natural surface water containing excessive phosphorus was collected, and its water quality was shown in Table 2.

Modification of copper tailings by calcium hydroxide (CCT)

$Ca(OH)_2$ suspensions with different concentrations were added into conical bottles containing CT respectively. The conical bottles were placed in a constant temperature water bath oscillator at 25 ℃ and oscillated at 150 rpm for 24 h. After standing and filtering, the solid was washed with pure water until the effluent pH was about 9.0–10.0, dried in the oven at 90–100 ℃ for 24 h, ground to 0.18 mm in diameter, and bagged.

The modification process of CT is shown in Fig. 1. CT modified with 0.05, 0.1, 0.2, 0.3, 0.4, 0.5 mol/L $Ca(OH)_2$ suspension were named CCT-0.05, CCT-0.1, CCT-0.2, CCT-0.3, CCT-0.4, CCT-0.5, respectively. The phosphate adsorbed CCT-0.4 was named CCT-0.4-P, and so on.

Toxicity leaching of CT and CCT

The solid leaching solution was prepared according to Solid waste, Sulfuric Acid and Nitric Acid method (HJ/T299-2007)[28]. First of all, 150–200 g samples were weighed and added to an extraction bottle with a capacity of 2 L. Then, according to the water content of the sample, the volume of the required extraction agent was calculated with a liquid–solid ratio of 10:1 (L/kg), and the mixed liquid extractant of concentrated sulfuric acid and concentrated nitric acid with a mass ratio of 2:1 was added to make the pH 3.20 ± 0.05. Subsequently, the bottle cap was tightly capped and fixed on the turnover oscillation device, the speed was adjusted to 30 ± 2 r/min, and the oscillation was 18 ± 2 h at 23 ± 2 ℃. Finally, the filtered filtrate is stored at 4 °C.

Composition	pH	Total phosphorus	NH_4-N^+	Total nitrogen	COD
Content	8.43	0.702 mg/L	33.714 mg/L	34.576 mg/L	30 mg/L

Table 2. Natural surface water quality.

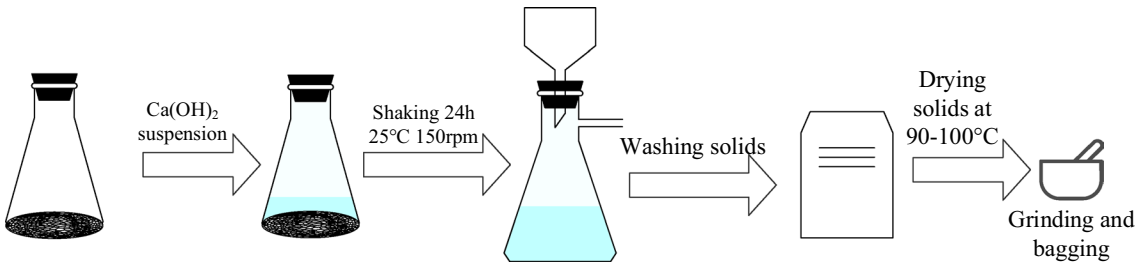

Fig. 1. The modification process of CT.

Phosphate sorption experiments

At a certain temperature, a certain concentration of phosphate solution is mixed with CCT according to a certain solid–liquid ratio, and the reaction is carried out at a certain pH value at a speed of 150 rpm for a certain time. After standing and filtering, the pH value and phosphate concentration of the filtrate were analyzed.

1. *Effect of solution pH.* 0.3 g CCT was added to a conical flask containing 100 ml phosphate (concentration 1 mg/L, pH (4–9)) and oscillated at 25 ℃ and 150 rpm for 1 h.
2. S*orption kinetic study.* 0.3 g CCT was added to a conical flask containing 100 ml phosphate (concentration 1 mg/L, pH 8) and oscillated at 25 ℃ and 150 rpm for 0 to 1 h. The pH value and phosphorus content of natural surface water were 8.43 and 0.702 mg/L respectively, and the reaction conditions were the same as those of simulated water.
3. *Effect of initial phosphate concentrations and contact temperature.* 0.3 g CCT was added to a conical flask containing 100 ml phosphate solution of varying concentrations (0.5–40 mg/L, pH 8) and oscillated at 150 rpm for 1 h at varying temperature (25–45 ℃).

Analytical method

According to ammonium molybdate spectrophotometry (GB 11893-89)[29], the concentration of phosphate in solution was determined by a visible spectrophotometer (722N, China) with a wavelength of 700 nm and a detection limit of 0.01 mg/L.

The phosphate removal rate was calculated according to Eq. (1).

$$R = \frac{C_0 - C_e}{C_0} \times 100\% \tag{1}$$

where C_0 and C_e (mg/L) are the initial concentrations and the equilibrium concentrations of phosphate respectively, and R is the phosphate removal rate.

The phosphate sorption capacity of CT/CCT (Q_t, mg/g) was calculated according to Eq. (2).

$$Q_t = (C_0 - C_t)V/M \tag{2}$$

where, C_t (mg/L) is the phosphate concentrations at the time t, V (L) is the volume of the phosphate solution and M (g) is the mass of the CT/CCT.

The determination methods used for different elements in identification for extraction toxicity tests are different. The concentration of potassium (K), sodium (Na), calcium (Ca) and magnesium (Mg) in the leaching solution was determined by an atomic absorption spectrophotometer (SP-35350AA, China). For the method, see GB 5085.3-2007[30] "Hazardous Waste Identification Standard—Extraction Toxicity Identification" catalog D. The concentration of mercury (Hg) in the leaching solution was determined by an atomic fluorescence photometer (AFS830, China). Methods refer to HJ 702-2014[31] "—Determination of Mercury, Arsenic, Selenium, Bismuth, Antimony in Solid Waste by Microwave Dissolution/Atomic Fluorescence Spectrometry". Other elements in the leaching solution were determined by inductively coupled plasma mass spectrometer (SUPEC7000, China), with reference to the microwave assisted acid digestion method in Appendix S of GB 5085.3-2007[30] "Hazardous Waste Identification Standard—Extraction Toxicity Identification".

Characterization method

The content of major oxides in CT was determined by X-ray fluorescence spectrometer (XRF, GF-V9, China). The BET surface area (S_{BET}), total pore volume and average pore size of CCT were determined by a specific surface area porosity analyzer (Samsung II.3020, China) based on N_2 adsorption–desorption method. The phase composition of adsorbents was analyzed by X-ray diffraction (XRD) spectrometer (DX-2700, China). The surface functional groups of CCT were studied by Fourier transform infrared spectrometer (ALPHA, Germany).

Results and discussion

Content of major oxides in CT

Table 3 shows the content of major oxides in CT.

As can be seen from Table 3, the main components of CT are SiO_2 and Al_2O_3, and the sum of their mass ratio is greater than 80%. At the same time, CT also contains trace amounts of heavy metals, and the sum of all heavy metal oxides mass ratio is less than 0.09%.

In order to explore the changes of CT before and after modification, elemental analysis of CCT-0.4 was also performed, and the results are shown in Table 4.

It can be seen from Table 4 that the calcium content of CCT-0.4 is significantly higher than that of CT, and the proportion of other elements is slightly reduced accordingly.

Composition	SiO_2	Al_2O_3	K_2O	Na_2O	MgO	SO_3	P_2O_5	Fe_2O_3	CaO	CuO	MnO	PbO	ZnO
Content (%)	63.88	16.37	4.38	2.12	0.99	0.93	0.66	0.79	0.46	0.07	0.01	0.004	0.002

Table 3. Content of major oxides in CT.

Composition	SiO_2	Al_2O_3	K_2O	Na_2O	MgO	SO_3	P_2O_5	Fe_2O_3	CaO	CuO	PbO	ZnO
Content (%)	59.62	13.92	4.38	1.84	0.99	0.91	0.63	0.61	2.86	0.04	0.004	0.002

Table 4. Content of major oxides in CCT-0.4.

As a solid waste, CT may contain toxic components, so toxic leaching tests were performed on CT and CCT-0.4, as shown in Tables 5 and 6.

It can be seen from Table 5 that according to the standard value for identification of leaching toxicity stipulated in "Hazardous Waste Identification Standard" (GB 5085.3-2007)[30], the concentration of each element is within the limit value.

As can be seen from Table 6, the leaching concentration of Ca^{2+} increased significantly in the modified CT, indicating that Ca was successfully loaded on CT, while the concentration of other ions did not change significantly.

Effect of pH on sorption

The effect of solution pH value on phosphate removal by CCT was studied and compared with that by CT. The results are shown in Fig. 2.

It can be clearly seen from Fig. 2 that all CCTs have higher phosphate removal than that of CT in the pH range studied (4–9). When the pH value of the solution was 4, the phosphate removal rate of CT was negative. This could be due to the fact that the phosphorus in CT (as shown in Table 3) dissolved under strong acid conditions and was released into the solution. The phosphate removal rate of CT increased with the increase of pH value of the solution, reaching a maximum of 68% at pH 9.

For CCT, on the one hand, phosphorus in CT may react with $Ca(OH)_2$ during the modification process; on the other hand, heavy metals including Cu^{2+} in CT also react with $Ca(OH)_2$ to form hydroxide precipitation.

$$Cu^{2+} + 2OH^{-} \rightarrow Cu(OH)_2 \tag{3}$$

At the same time, with the increase of $Ca(OH)_2$ concentration (0.05–0.4 mol/L), the phosphate removal rate of CCT-0.05 to CCT-0.4 also increased. When the concentration of $Ca(OH)_2$ was low (0.05–0.1 mol/L), the phosphorus removal of CCT-0.05 and CCT-0.1 increased with the increase of solution pH under acidic condition, and slightly decreased with the increase of solution pH under alkaline condition. This may be due to the deprotonation of the adsorbent surface in an alkaline environment, which weakened the electrostatic attraction between the adsorbent and the adsorbent, and increased the repulsive force between them. When the concentration of calcium hydroxide was relatively high (0.3–0.4 mol/L), the phosphorus removal of CCT-0.3 and CCT-0.4 was basically unchanged under acidic conditions, but it increases with the increase of solution pH under alkaline conditions, especially the phosphorus removal of CCT-0.4 was nearly 100% at pH 9. This may be due to the high concentration of OH^- in the solution under alkaline conditions, which makes Ca^{2+} combine with phosphate to form $Ca_5(PO_4)_3(OH)$ precipitation, as shown in Eq. (4). The precipitation reaction compensated for the reduced electrostatic attraction caused by deprotonation, so the phosphorus removal rate increased with increasing pH value.

Element	Hg	K	Ca	Na	Mo	Mg	B	Be	Al
Concentration (mg/L)	$1.9*10^{-4}$	0.22	15.0	0.52	0.002	2.06	0.11	0.001	0.34
Element	V	Cr	Mn	Fe	Co	Ni	Cu	Zn	As
Concentration (mg/L)	$8.0*10^{-5}$	0.01	0.12	0.50	0.10	0.07	16.7	0.98	0.012
Element	Se	Sr	Ag	Cd	Pb	Sb	Tl		
Concentration (mg/L)	0.01	0.01	0.03	0.009	0.01	$<1.5*10^{-4}$	0.0001		

Table 5. Toxicity leaching test results for all elements in CT.

Element	Hg	K	Ca	Na	Mo	Mg	B	Be	Al
Concentration (mg/L)	$1.9*10^{-4}$	0.22	283	0.52	0.002	2.05	0.11	0.001	0.33
Element	V	Cr	Mn	Fe	Co	Ni	Cu	Zn	As
Concentration (mg/L)	$8.0*10^{-5}$	0.01	0.12	0.49	0.10	0.07	16.7	0.97	0.012
Element	Se	Sr	Ag	Cd	Pb	Sb	Tl		
Concentration (mg/L)	0.01	0.01	0.03	0.009	0.01	$<1.5*10^{-4}$	0.0001		

Table 6. Toxicity leaching test results for all elements in CCT-0.4.

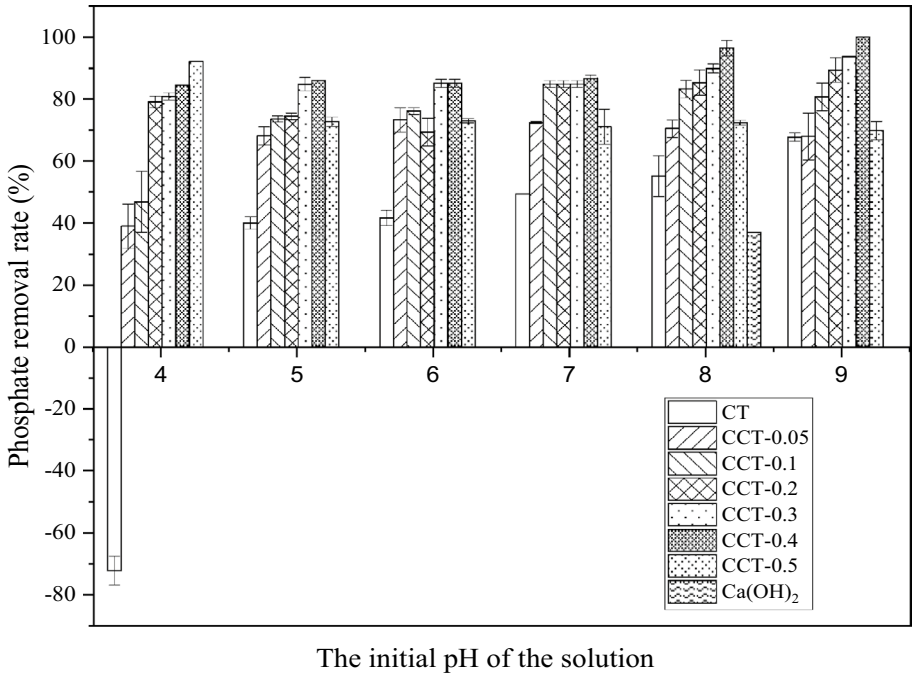

Fig. 2. Effect of pH on sorption (initial phosphate concentration 1 mg/L; CCT 3 g/L; contact temperature 25 ℃; contact time 1 h).

$$5Ca^{2+} + 3PO_4^{3-} + OH^- \rightarrow Ca_5(PO_4)_3(OH) \quad (4)$$

As for CCT-0.5, it has the highest phosphate removal rate (92%) at pH 4. Under alkaline conditions, the phosphorus removal rate decreased slightly with the increase of pH value, and the trend was similar to CCT-0.05. On the one hand, the deprotonation of the adsorbent surface may lead to the decrease of phosphorus sorption rate. On the other hand, the high turbidity of 0.5 mol/L calcium hydroxide suspension resulted in reduced calcium adhesion on CT.

In order to investigate the interaction between CT and $Ca(OH)_2$, $Ca(OH)_2$ powder was used instead of CCT to remove phosphate from water under the same reaction conditions. The results show that the removal rate of phosphate by $Ca(OH)_2$ was only 37%, indicating that there is a synergistic effect between CT and $Ca(OH)_2$ in the process of phosphate removal in water by CCT.

The above results show that when the concentration of modifier calcium hydroxide was low, the amount of Ca^{2+} attached to CT was also low, and the competitive sorption of OH^- and PO_4^{3-} in alkaline solutions was dominant[24]. When the concentration of modifier calcium hydroxide was higher, the amount of Ca^{2+} attached to CT was also higher. Under alkaline conditions, $Ca_5(PO_4)_3(OH)$ can compensate for competitive sorption, as shown in Eq. (4).

To investigate the electrostatic attraction role in the removal process, the zeta potential of different adsorbents, and the result was shown in Fig. 3.

As can be seen from Fig. 3, the point of zero charge (pH_{PZC}) for CT, CCT-0.1, CCT-0.2, CCT-0.3, CCT-0.4, CCT-0.5 are 4.54, 5.30, 5.00, 4.72, 4.52, 5.08, 4.82 respectively, indicating that pH_{PZC} has slightly changed during modification of CT. The zeta potential of CT and CCTs show the same trend with pH value. The CT removal rate increased with increasing pH value, indicating the removal process involved more than electrostatic attraction. It may be because Al^{3+} in CT (as shown in Table 3) reacts with phosphate under alkaline conditions, as shown in Eq. (5). Generally, $Al(OH)_3$ begins to be generated in the pH 3.3–3.4 range and completes at pH 5.2. However, it begins to dissolve at pH = 7.8 and completely dissolves at pH = 10.8[32,33].

$$Al^{3+} + H_2PO_4^- + OH^- \rightarrow H_2O + AlPO_4 \quad (5)$$

However, the removal rate of phosphate by CCT decreased when the initial solution pH value was above the $pH_{PZC,}$ but it is not a perfect fit. This may be due to the fact that the reaction between Al^{3+} and Ca^{2+} and phosphorus is enhanced with increasing pH value, which counteracts the decrease in phosphate removal brought about by weaker electrostatic repulsion. The disparity between CT and CCT could be attributed to the swift increase in the pH level of the solution during the reaction of CCT and phosphate solution, leading to the rapid dissolution of $Al(OH)_3$.

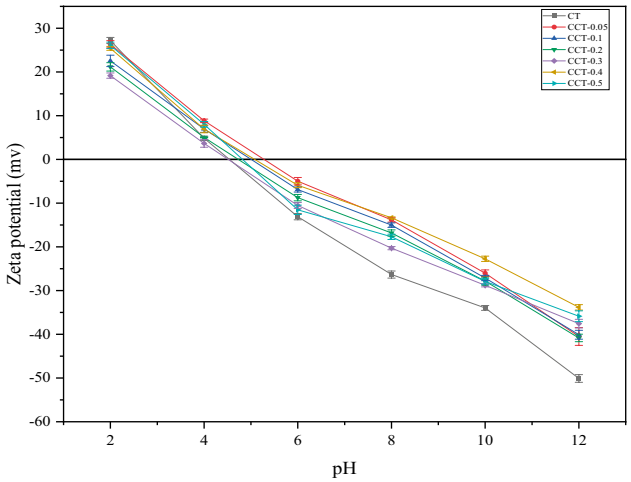

Fig. 3. The zeta potential of CT and CCT.

Change of solution pH value before and after removal

In order to further study the mechanism of phosphate removal by CT and CCT, the change of solution pH value before and after removal was analyzed, as shown in Fig. 4.

As can be seen from Fig. 4, in the pH range studied (4–9), the pH value of the solution removal by CT was always between 6 and 7.5, possibly due to the pH regulation effect of phosphate. Phosphate can keep the solution pH stable within a certain range, and its buffer range is within pH 5–9[34]. The pH value after phosphate removal by CCT was all higher than the pH value before removal. This may because during the sorption process, OH^- attached to the CCT surface was released into solution. At the same time, Ca^{2+} was released into the solution.

Combined with the fact that $Ca(OH)_2$ alone has poor phosphorus removal efficiency, it is speculated that the sorption mechanism can be divided into two parts. Some phosphates react with Ca^{2+} dissolved in solution to form $Ca_3(PO_4)_2$, and the other part of phosphates are first physically adsorbed to the surface of CCT, and then react with Ca^{2+} attached to the surface of CCT to form $Ca_3(PO_4)_2$.

$$Ca^{2+} + HPO_4^{2-} + OH^- \rightarrow Ca_3(PO_4)_2 + H_2O \quad (6)$$

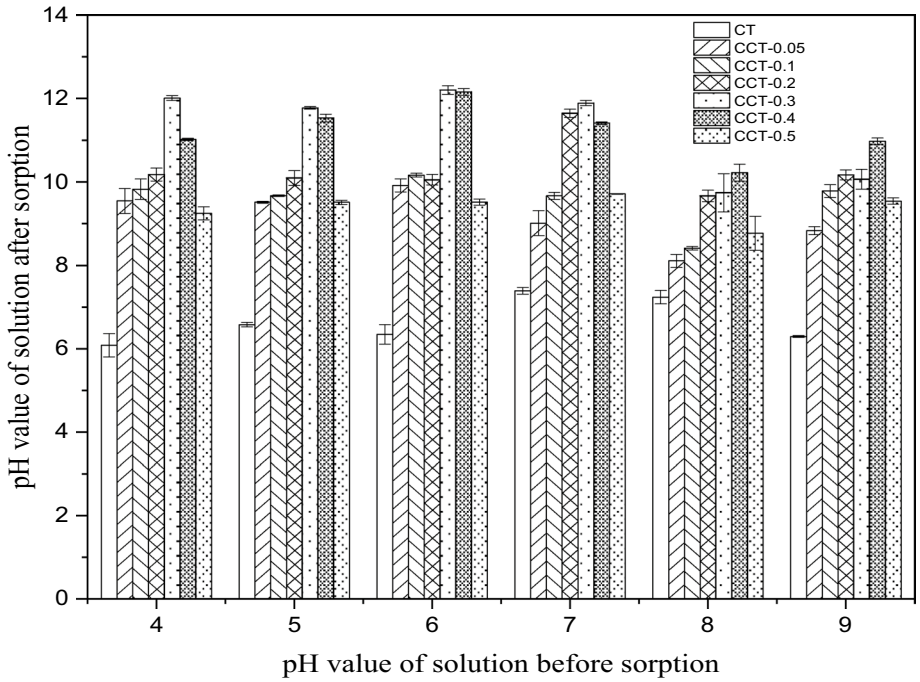

Fig. 4. pH value of solution before and after sorption.

Under acidic conditions, the surface of the adsorbent was positively charged due to protonation, as shown in Eq. (7), facilitating electrostatic gravitational interaction with phosphates in solution, as shown in Eq. (8).

$$\text{Ca - OH} + \text{H}^+ \leftrightarrow \text{Ca - OH}_2^+ \tag{7}$$

$$\text{Ca - OH}_2^+ + \text{H}_2\text{PO}_4^- \leftrightarrow (\text{Ca - OH}_2)^+\left(\text{H}_2\text{PO}_4^-\right) \tag{8}$$

However, the precipitation between Ca^{2+} and phosphate is more favorable under alkaline conditions, compensating for the reduced phosphate removal rate caused by deprotonation. As a result, phosphate removal increases rather than decreases with increasing pH. It can be seen from the experimental results that electrostatic attraction and surface precipitation play a key role in the process of phosphorus removal. With the increase of pH, the electrostatic attraction effect weakens and the precipitation reaction effect increases.

As can be seen from the above experimental results, CCT-0.4 has the highest phosphorus removal efficiency, so the subsequent experiments mainly study CCT-0.4.

The contents of various elements in the solution after phosphate sorption by CCT-0.4 at pH 8 were studied, and the results were shown in Table 7.

As can be seen from Table 7, when the pH value of the solution is 8, the content of all heavy metal elements measured meets the limit requirements of the Class III standard of the Environmental Quality Standard for surface water (GB3838-2002)[35], indicating that $Ca(OH)_2$ has varying degrees of fixing effect on most metal ions.

Sorption kinetic study

Kinetic studies were conducted, and the results were shown in Fig. 5. The phosphate sorption rate of CCT-0.4 increased rapidly in the first 5 min, but then gradually slowed down and reached equilibrium at 40 min.

Pseudo-first-order:

$$q_t = q_e(1 - e^{-k_1 t}) \tag{9}$$

Pseudo-first-order:

Element	Hg	K	Ca	Na	Mo	Mg	B	Be	Al
Concentration (mg/L)	$1.72*10^{-4}$	0.22	7.6	0.52	0.002	0.76	0.10	0.001	0.12
Element	V	Cr	Mn	Fe	Co	Ni	Cu	Zn	As
Concentration (mg/L)	$7.1*10^{-5}$	0.01	0.09	0.30	0.06	0.01	0.81	0.58	0.01
Element	Se	Sr	Ag	Cd	Pb	Sb	Tl		
Concentration (mg/L)	0.01	0.01	0.03	0.005	0.01	$1.0*10^{-4}$	0.0001		

Table 7. The concentration of elements in the solution after phosphate sorption by CCT-0.4 at pH 8.

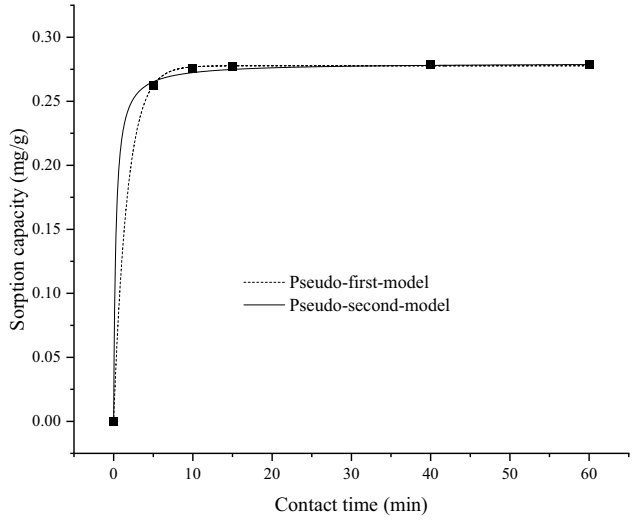

Fig. 5. Kinetic results of sorption of simulated water containing phosphorus (initial phosphate concentration 1 mg/L; CCT 3 g/L; contact temperature 25 ℃; contact time 0–60 min).

$$q_t = \frac{q_e^2 k_2 t}{1 + q_e k_2 t} \tag{10}$$

where t is time (min), q_t (mg/g) and q_e (mg/g) are sorption capacity of adsorbents at time t and at equilibrium, respectively. k_1 (min^{-1}) and k_2 (g/(mg·min)) are rate constants, respectively. k_1 (min^{-1}) and k_2 (g/mg·min) are rate constants respectively.

The correlation coefficient (R^2) of the two models shown in Table 8 indicates that both the pseudo-first-order model and the pseudo-second-order model can fit the sorption kinetics well. The pseudo-second order describes the CCT sorption process under the control of chemisorption mechanism[36] and the kinetic fitting results also indicate that the sorption process is mainly chemisorption, which is also consistent with the speculation.

Since the target of the adsorbent is always the natural water, natural water is collected for the experiment, and the results are shown in Fig. 6.

It can be seen that the sorption amount of phosphorus in natural surface water by CCT-0.4 is slightly smaller than that in simulated water. This may be because COD and nitrate in natural water (Table 2) compete with phosphate for the sorption sites of CCT-0.4.

At the same time, there was no significant difference in the sorption amount of phosphorus between 60 min and 24 h, indicating that CCT-0.4 basically reached sorption equilibrium at 60 min. The kinetic fitting results of phosphorus sorption by CCT-0.4 in natural surface water are shown in Table 9.

Similar to the simulated phosphorus water sorption results, the pseudo-second-order kinetic model is in good agreement with the experimental results, indicating that CCT-0.4 chemisorption is dominant in both simulated water and natural surface water.

Sorption isotherm study

To further study the phosphate sorption by CCT-0.4, two sorption isotherms models, Langmuir and Freundlich, were used to describe the reaction.

Langmuir model:

Pseudo-first-order			Pseudo-second-order		
k_1(min^{-1})	q_e	R^2	k_2 (g/(mg·min))	q_e	R^2
0.58	0.28	0.99	12.86	0.28	0.99

Table 8. Parameters of sorption kinetic.

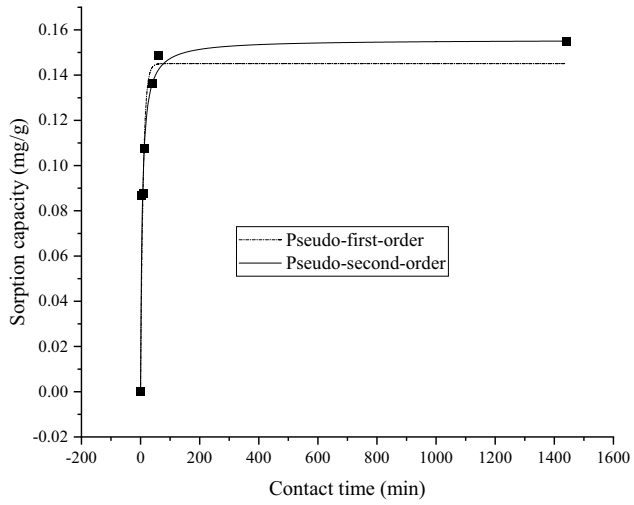

Fig. 6. Kinetic results of sorption of natural surface water containing phosphorus (phosphate concentration 0.702 mg/L; CCT 3 g/L; contact temperature 25 ℃; pH 8.43; contact time 0–1440 min).

Pseudo-first-order			Pseudo-second-order		
k_1(min^{-1})	q_e	R^2	k_2 (g/(mg·min))	q_e	R^2
0.11	0.15	0.94	1.13	0.16	0.98

Table 9. Parameters of sorption kinetic.

$$q_e = \frac{K_1 C_e q_m}{1 + K_1 C_e} \tag{11}$$

Freundlich model:

$$q_e = K_2 C_e^{\frac{1}{n}} \tag{12}$$

where q_e (mg/g) is the equilibrium sorption capacity, and q_m (mg^{-1}) represented the maximum sorption capacity. *Ce* (mg/L) represented the phosphate concentration at sorption equilibrium. K_1 (L/mg) and K_2 (mg/g) represent the sorption equilibrium constant and the Freundlich constant, respectively, *1/n* indicates the sorption strength.

The sorption isotherm results are shown in Fig. 7. According to the correlation coefficient R^2, Langmuir model can fit the sorption process better than Freundlich model at different temperatures, indicating that the sorption process belongs to monolayer chemisorption[37], which is in accordance with the kinetic results.

Table 10 shows that the value of *1/n* at different temperatures ranges from 0.1 to 0.5, indicating that the sorption process is feasible.

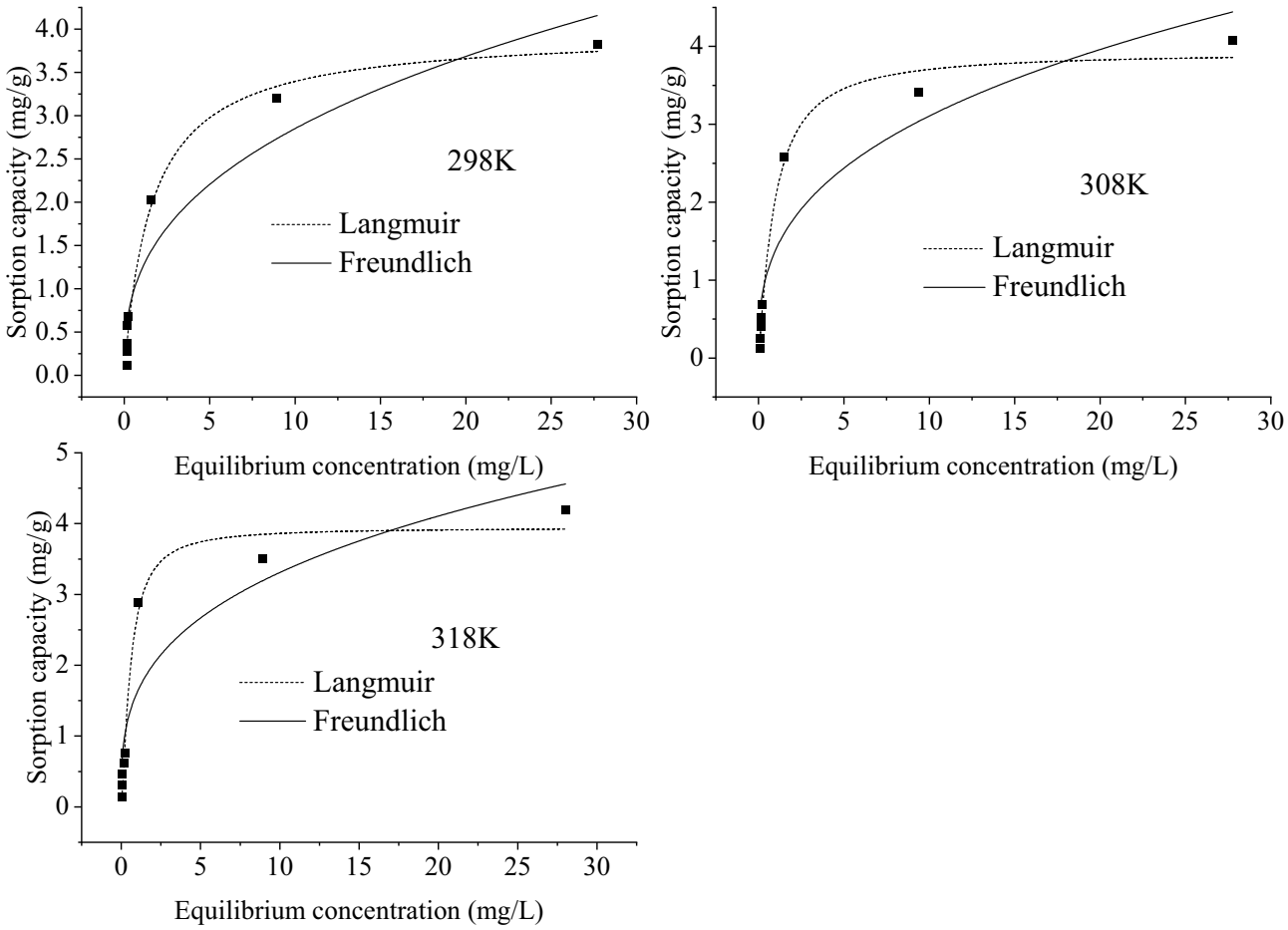

Fig. 7. The results of sorption isotherm (initial phosphate concentration 0.5–40 mg/L; CCT 3 g/L; contact temperature 25–45 ℃; contact time 1 h).

Model	Langmuir			Freundlich		
parameters	K_1 (L/mg)	q_m (mg/g)	R^2	K_2 (mg/g)	*1/n*	R^2
25 ℃	0.62123	3.9817	0.9858	1.2154	0.3703	0.9213
35 ℃	1.1014	3.9278	0.9896	1.3868	0.3503	0.8962
45 ℃	2.0973	3.9415	0.9846	1.6161	0.3113	0.8727

Table 10. Parameters of sorption isotherm.

Sorption thermodynamics study

Using the Gibbs free energy (ΔG), entropy change (ΔS), and enthalpy change (ΔH) to describe the thermodynamic behavior of sorption, the Van't Hoff equation is obtained, as shown in the equations (Eqs. (13)–(15)[38–40].

$$K_d = \frac{q_e}{C_e} \tag{13}$$

$$\Delta G = \Delta H - T\Delta S \tag{14}$$

$$\ln K_d = \frac{\Delta S}{R} - \frac{\Delta H}{RT} \tag{15}$$

where K_d is the equilibrium sorption distribution constant, ΔG (kJ/mol) is the free energy change value of the sorption process, ΔS (J/(K·mol)) is the sorption entropy change of the sorption process, ΔH (kJ/mol) is the enthalpy change of the sorption process, C_e (mg/L) is the phosphate concentration at sorption equilibrium, and R is the thermodynamic constant (8.314 J/(K·mol)), and T is the absolute temperature (K).

According to Van't Hoff Eq. (15), $1/T$ was plotted by ln$K$, and Fig. 8 was obtained. The apparent enthalpy change ΔH and apparent entropy change ΔS of sorption reaction were calculated respectively according to slope and intercept, and the results are shown in Table 11.

The calculation results in Table 11 show that at the three temperatures studied, the apparent free energy change ΔG of the sorption reaction of phosphate by the adsorbent CCT-0.4 is less than 0, indicating the spontaneity of the sorption reaction.

In general, the ΔH range of physical sorption is 0–20 kJ/mol and the chemisorption range is 80–300 kJ/mol[41]. The ΔH of phosphate sorption in this study was 53.54 kJ/mol, indicating that the sorption process includes physical sorption and chemisorption, which is exactly consistent with the experimental results, that is, electrostatic attraction belongs to physical sorption, surface precipitation belongs to chemisorption.

The apparent entropy change ΔS (182.82 J/(K·mol)) indicates that the entropy of the sorption process increases ($\Delta S > 0$), which means that the sorption of phosphoric acid increases the disorder of CCT-0.4.

Combining with the results of thermodynamic and kinetic studies, it can be inferred that the main mechanism of phosphate sorption by CCT is chemisorption. This result is similar to phosphate sorption in Florida Bay sediments. Phosphate sorption in CCT-0.4 and Florida Bay sediments is primarily dependent on calcium, and both exhibit initial rapid chemisorption and production hydroxyapatite[42]. It can be seen from Fig. 8 that the K_d value also increases with the increase of temperature, which is consistent with the trend mentioned in previous studies[43]. However, it can be seen from Fig. 7 that under different concentrations, the sorption capacity only increases slightly or remains basically unchanged with the increase of temperature, and according to the

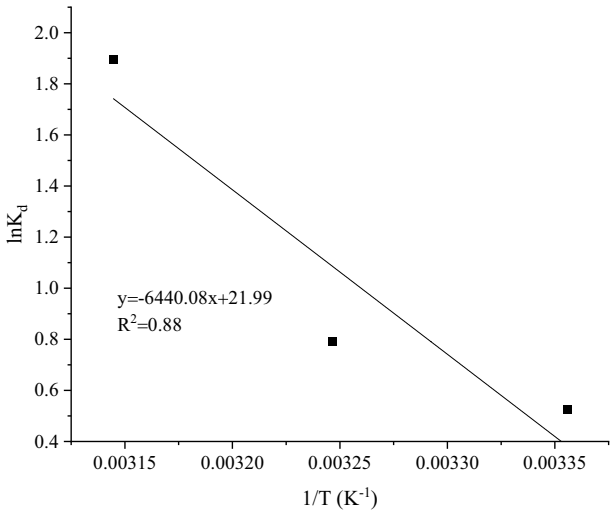

Fig. 8. Van't Hoff plot for phosphate sorption on CCT-0.4.

T (K)	ΔG (kJ/mol)	ΔH (kJ/mol)	ΔS (J/(K·mol))
298	− 0.94	53.54	182.82
308	− 2.77		
318	− 5.26		

Table 11. Thermodynamics data of phosphate sorption on CCT-0.4.

isotherm fitting results, the q_m at different temperatures remains basically unchanged, indicating that the influence of temperature on the phosphorus sorption on CCT-0.4 is not significant.

Table 12 summarizes the phosphate sorption capacity of various calcium-modified adsorbents. Table 12 shows that, in contrast, CCT can achieve a better removal rate in a shorter period of time. The small sorption capacity of CCT-0.4 is due to the low initial phosphate concentration. Therefore, in the removal of low concentration phosphate, CCT-0.4 is a better choice.

Characterization of adsorbent

BET analysis of CT and CCT-0.4

The N_2 sorption and desorption curves and pore distribution of CT and CCT-0.4 are shown in Fig. 9.

As shown in Fig. 9, the N_2 sorption capacity of CCT-0.4 is higher than that of CT, and the contribution of pores above 4 nm to the pore volume increases.

According to the IUPAC classification, the N_2 sorption and desorption curves of CT and CCT-0.4 are type IV isotherms with H3 hysteresis loops. When $P/P_0 < 0.46$, the sorption capacity of N_2 increased with the increase of relative pressure, and the sorption curve coincided with the desorption curve, indicating that the sorption belongs to monolayer sorption[48].

Adsorbent	Initial pH	sorption capacity (mg/g)	Contact time (h)	Initial phosphate concentration (mg/L)
Ca-biochar[44]	11	44.04	24	50
Ca-clinoptilolite[45]	7	2.91	120	10
Ca-LDHs[46]	7	132.5	24	75
La-Ca/Fe-LDH[47]	7	109.94	24	50
This study	8	0.28	0.67	1

Table 12. Phosphate sorption capacities of various adsorbents.

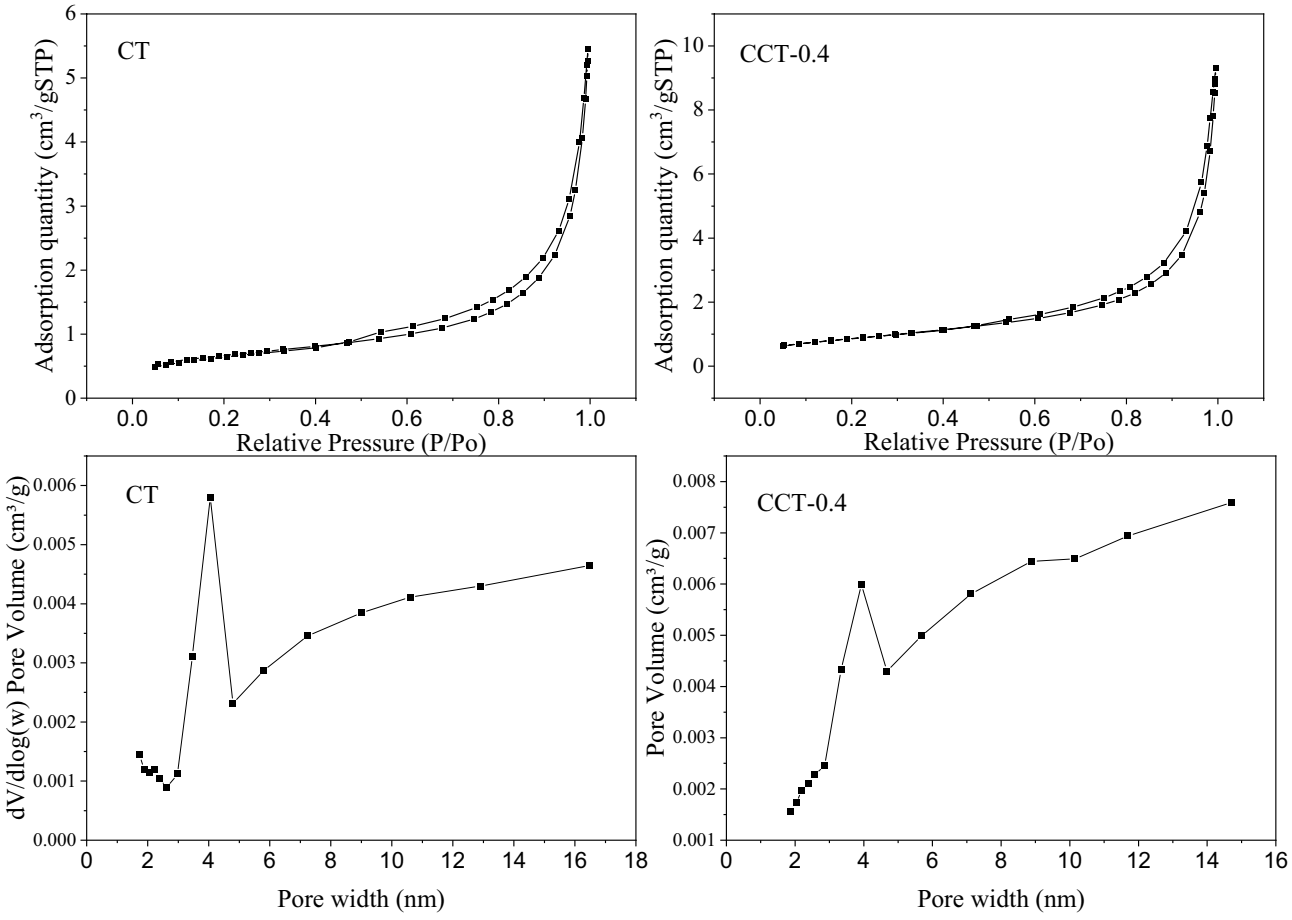

Fig. 9. The N_2 sorption and desorption curves and pore distribution diagram of CT and CCT-0.4.

It can also be seen from Fig. 9 that the aperture of CCT-0.4 is wider than that of CT. BET results showed that the specific surface area of CCT-0.4 and CT were 3.12 and 2.28 m^2/g respectively, and their pore volume were 0.005 and 0.003 cm^3/g, respectively. The specific surface area and pore volume of CCT-0.4 are higher than those of CT, which may determine the sorption capacity of CCT-0.4 is stronger than that of CT[49].

XRD analysis of adsorbents

The crystal transformation before and after CT modification was studied by XRD. The result is shown in Fig. 10.

It can be seen from Fig. 10 that the characteristic peaks intensity of SiO_2 in CCT is weaker than that in CT, while the characteristic peak intensity of calcium is stronger than that in CT, increasing from CCT-0.05 to CCT-0.4.

The characteristic peaks of CCT-0.2 at $2\theta = 27.63°$, CCT-0.3 at $2\theta = 26.66°$, 28.02°, 50.13°, CCT-0.4 at $2\theta = 20.88°$, 26.64°, 27.94°, 42.45° and CCT-0.5 at $2\theta = 26.69°$ belong to $CaAl_2Si_2O_8{\cdot}4H_2O$, and the peak intensity is the highest at CCT-0.4 and the lowest at CCT-0.5, which is just consistent with the experimental results.

The crystal transformation before and after phosphate sorption by CCT was studied by XRD. The result is shown in Fig. 11.

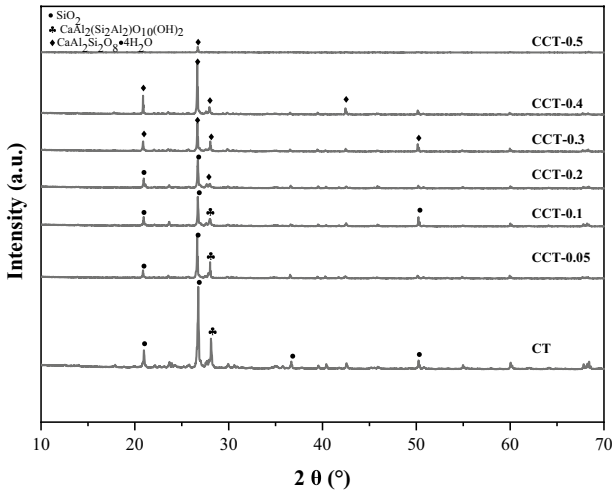

Fig. 10. XRD analysis of CT before and after modification.

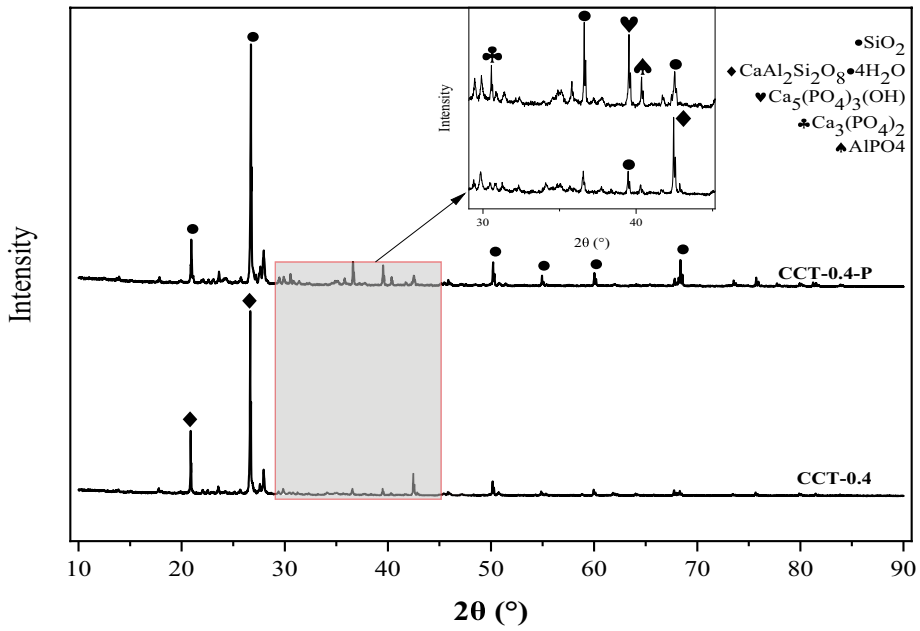

Fig. 11. The XRD of CCT-0.4 before and after phosphate sorption.

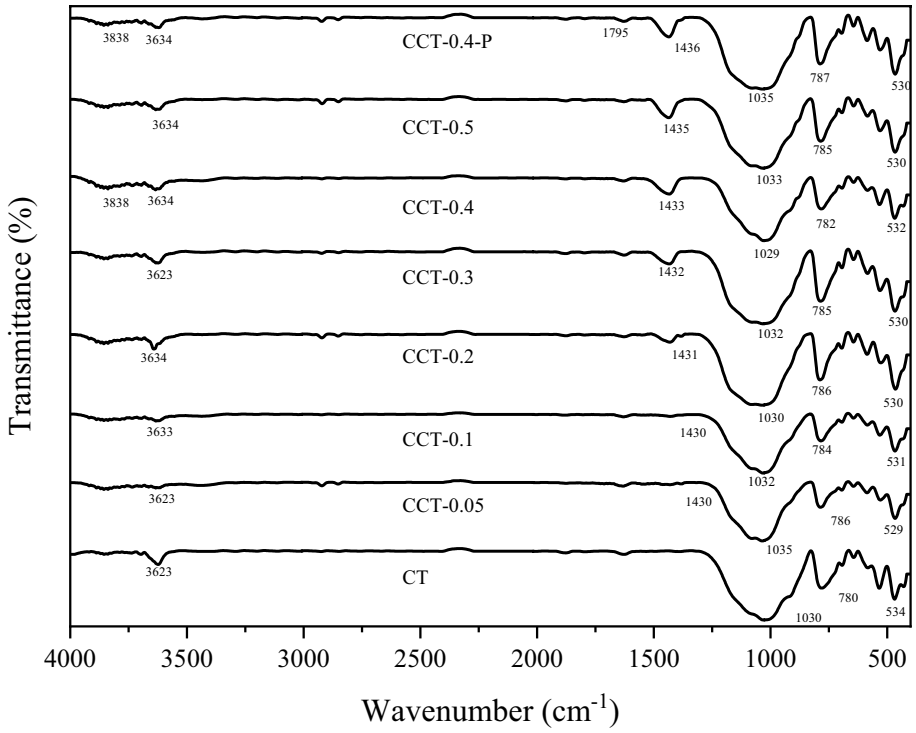

Fig. 12. FTIR analysis of adsorbents.

Figure 11 shows the crystal phase changes of CCT-0.4 before and after phosphate sorption. The diffraction peaks observed by CCT-0.4 at 2θ = 20.88°, 26.64°, 27.94°, and 42.45° belong to $CaAl_2Si_2O_8{\cdot}4H_2O$. After phosphate sorption, the CCT-0.4-P showed that the typical peaks of $CaAl_2Si_2O_8{\cdot}4H_2O$ almost disappeared. A new $Ca_3(PO_4)_2$ diffraction peak appeared at 2θ = 30.552°[50], and new $Ca_5(PO_4)_3(OH)$ diffraction peaks at 2θ = 35.804° and 39.553°[51], indicating that the calcium participated in the precipitation reaction, as shown in equations (Eq. (4), (6)). Meanwhile, a new $AlPO_4$ diffraction peak occurred at 2θ = 40.35°, illustrating the Al^{3+} participated in the precipitation reaction.

It can be inferred that surface precipitation is the main mechanism of phosphorus removal. Therefore, CCT-0.4 has the best phosphorus removal effect because it has the highest amount of calcium attached.

FTIR analysis of adsorbents.

The FTIR spectra of CT, CCT and CCT-0.4-P are shown in Fig. 12.

As can be seen from Fig. 12, there is no significant difference between CT and CCT spectra. The sorption peaks near 530 cm^{-1} and 780 cm^{-1} represents the flexural vibration of Si–O, and the sorption peak near 1030 cm^{-1} represents the tensile parallelism of Si–O–Si.

The spectral difference between CCT and CCT-0.4-P is not obvious. After phosphate sorption, the peak redshift of CCT-0.4 at 1029 cm^{-1} to 1035 cm^{-1} is caused by O-P tensile vibration[46], indicating that phosphate has been adsorbed by CCT-0.4.

Conclusions

The natural accumulation of copper tailings (CT) occupies a large area of land. Considering the resource properties and waste properties of CT, effective use of CT can not only make use of the resources in it, but also save land and reduce the harm to human health. In this study, $Ca(OH)_2$ were used to modify CT to fix the heavy metals and improve the removal capacity of phosphate. The results showed that when the concentration of modifier $Ca(OH)_2$ was 0.4 mol/L, the initial concentration of phosphate 1 mg/L and the solution pH 8, the phosphate removal rate of CCT was 96.5%. The mechanism study shows that the process of CCT removal of phosphate involves electrostatic sorption and surface precipitation, and there is a synergistic effect between CT and calcium hydroxide. The XRD patterns of CCT-0.4 and CCT-0.4-P showed that $Ca_3(PO_4)_2$, $Ca_5(PO_4)_3(OH)$ and $AlPO_4$ exist in CCT after phosphate removal, indicating that surface precipitation occurs during the removal process. In summary, the removal mechanism of phosphate by CCT is mainly electrostatic attraction and surface precipitation.

Data availability

All data generated or analyzed during the study are included in the published article and its Supplementary Information file.

Received: 31 December 2023; Accepted: 27 August 2024
Published online: 02 September 2024

References

1. Wujcicki, L. et al. Cerium(IV) chitosan-based hydrogel composite for efficient adsorptive removal of phosphates(V) from aqueous solutions. *Sci. Rep.* https://doi.org/10.1038/s41598-023-40064-1 (2023).
2. Huang, Y. et al. Modified biochar for phosphate adsorption in environmentally relevant conditions. *Chem. Eng. J.* **380**, 122375. https://doi.org/10.1016/j.cej.2019.122375 (2020).
3. Wang, Z., Shen, D., Shen, F. & Li, T. Phosphate adsorption on lanthanum loaded biochar. *Chemosphere* **150**, 1–7. https://doi.org/10.1016/j.chemosphere.2016.02.004 (2016).
4. Silva, M. & Baltrusaitis, J. A review of phosphate adsorption on Mg-containing materials: Kinetics, equilibrium, and mechanistic insights. *Environ. Sci. Water Res. Technol.* **6**, 3178–3194. https://doi.org/10.1039/d0ew00679c (2020).
5. Yi, M. & Chen, Y. Enhanced phosphate adsorption on Ca-Mg-loaded biochar derived from tobacco stems. *Water Sci. Technol.* **78**, 2427–2436. https://doi.org/10.2166/wst.2019.001 (2018).
6. Liu, Y. Current situation of eutrophication of water body at home and abroad and research progress of phosphate accumulating bacteria. *Jiangsu Agric. Sci.* **49**, 26–35. https://doi.org/10.15889/j.issn.1002-1302.2021.09.005 (2021).
7. Luo, H. et al. Key roles of the crystal structures of MgO-biochar nanocomposites for enhancing phosphate adsorption. *Sci. Total Environ.* **766**, 142618. https://doi.org/10.1016/j.scitotenv.2020.142618 (2021).
8. Zhang, L. et al. Phosphate adsorption on lanthanum hydroxide-doped activated carbon fiber. *Chem. Eng. J.* **185**, 160–167. https://doi.org/10.1016/j.cej.2012.01.066 (2012).
9. Yang, Y. et al. An innovative lanthanum carbonate grafted microfibrous composite for phosphate adsorption in wastewater. *J. Hazard. Mater.* **392**, 121952. https://doi.org/10.1016/j.jhazmat.2019.121952 (2020).
10. Li, J. et al. Investigation into lanthanum-coated biochar obtained from urban dewatered sewage sludge for enhanced phosphate adsorption. *Sci. Total Environ.* **714**, 136839. https://doi.org/10.1016/j.scitotenv.2020.136839 (2020).
11. Shin, H., Tiwari, D. & Kim, D.-J. Phosphate adsorption/desorption kinetics and P bioavailability of Mg-biochar from ground coffee waste. *J. Water Process Eng.* **37**, 101484. https://doi.org/10.1016/j.jwpe.2020.101484 (2020).
12. Gao, W. & Gao, X. Study of pollution status and treatment of re-election tailings from copper smelting slag. *Nonferrous Metals (Extractive Metallurgy)* https://doi.org/10.3969/j.issn.1007-7545.2014.11.018 (2014).
13. Zhang, H. et al. Utilization status and prospect of copper tailings resources. *Modern Min.* **33**, 127–131. https://doi.org/10.3969/j.issn.1674-6082.2017.01.031 (2017).
14. Wang, Y., Zhang, J. & Wang, L. Critical issues and countermeasures towards China's recycling utilization of mining solid wastes in the New Normal Economy. *China Min. Mag.* **25**, 69–73+91. https://doi.org/10.3969/j.issn.1004-4051.2016.09.016 (2016).
15. Xu, J. Removal of phosphate from aqueous solution by copper tailings. *Anhui Univ.* https://doi.org/10.7666/d.Y2320631 (2013).
16. Xiao, L. & Zhu, J. Study on hydration properties of composite cementitious materials based on copper tailing powders. *Non-Metallic Miners* **43**, 61–63. https://doi.org/10.3969/j.issn.1000-8098.2020.02.016 (2020).
17. Ma, D. Preparation and adsorption properties of porous ceramics from copper railings. *Ceramics* https://doi.org/10.19397/j.cnki.ceramics.2019.09.004 (2019).
18. Tan, J. The use of modificatory copper oxidemain tailing and cattle manure in removing phosphorus and dye from solution. *Anhui Univ.* https://doi.org/10.7666/d.d202724 (2008).
19. Jin, H. et al. A novel lanthanum-modified copper tailings adsorbent for phosphate removal from water. *Chemosphere* **281**, 130779. https://doi.org/10.1016/j.chemosphere.2021.130779 (2021).
20. Kumar, P. S., Korving, L., Keesman, K. J., van Loosdrecht, M. C. & Witkamp, G.-J. Effect of pore size distribution and particle size of porous metal oxides on phosphate adsorption capacity and kinetics. *Chem. Eng. J.* **358**, 160–169. https://doi.org/10.1016/j.cej.2018.09.202 (2019).
21. Li, J., Wang, P., Wan, S. & Chen, R. High porosity biochar and its treatment of phosphate in wastewater. *Acta Materiae Compositae Sinica* https://doi.org/10.13801/j.cnki.fhclxb.20230131.001 (2023).
22. Zhou, R. et al. Effect of heating temperature and time on the phosphate adsorption capacity of thermally modified copper tailings. *Water Sci. Technol.* **77**, 2668–2676. https://doi.org/10.2166/wst.2018.230 (2018).
23. Kong, L., Xue, F., Chen, L., Sun, Q. & Yang, L. Adsorption of phosphate on copper mine tailing samples. *Environ. Pollut. Control* https://doi.org/10.3969/j.issn.1001-3865.2008.05.006 (2008).
24. Nie, G. et al. A millimeter-sized negatively charged polymer embedded with molybdenum disulfide nanosheets for efficient removal of Pb (II) from aqueous solution. *Chin. Chem. Lett.* **32**, 2342–2346. https://doi.org/10.1016/j.cclet.2020.12.014 (2021).
25. Yuan, P. Study on comprehensive utilization of copper tailings resources in a place in Anhui province. *Min. Eng.* **21**, 61–65. https://doi.org/10.16672/j.cnki.kygc.2023.02.013 (2023).
26. Shi, X., Yi, Y., Anivar, S. & Li, C. Study on the synergistic activation and cementing and hydration properties of tailings sodium salt ball milling. *China Min. Mag.* **32**, 108–117. https://doi.org/10.12075/j.issn.1004-4051.2023.03.004 (2023).
27. Fen, Y., Liang, H., Zhang, H. & Liu, M. Experimental study on flotation process of a mixed low-grade copper tailings from Yunnan. *Nonferrous Metals (Miner. Process. Sect.)* https://doi.org/10.3969/j.issn.1671-9492.2022.06.008 (2022).
28. Ministry of Ecology and Environment of the People's Republic of China *Solid waste-Extraction procedure for leaching toxicity-Sulphuric acid & nitric acid method*, https://www.mee.gov.cn/ywgz/fgbz/bz/bzwb/jcffbz/200704/t20070418_102859.shtml (2007).
29. Ministry of Ecology and Environment of the People's Republic of China *Water quality-Determination of total phosphorus-Ammonium molybdate spectrophotometric method*, https://www.mee.gov.cn/ywgz/fgbz/bz/bzwb/jcffbz/199007/t19900701_67131.shtml (1990).
30. Ministry of Ecology and Environment of the People's Republic of China *Identification standards for hazardous wastes-Identification for extraction toxicity*, https://www.mee.gov.cn/ywgz/fgbz/bz/bzwb/gthw/wxfwjbffbz/200705/t20070522_103957.shtml (2007).
31. Ministry of Ecology and Environment of the People's Republic of China *Solid Waste—Determination of Mercury, Arsenic, Selenium, Bismuth, Antimony—Microwave Dissolution/Atomic Fluorescence Spectrometry*, https://www.mee.gov.cn/ywgz/fgbz/bz/bzwb/jcffbz/201409/t20140912_288936.shtml (2014).
32. Gao, L., Quan, L., Liu, T., Xing, R. & Li, J. Combined determination of yttrium and aluminum. *Metal. Funct. Mater.* **30**, 85–88. https://doi.org/10.13228/j.boyuan.issn1005-8192.20230006 (2023).
33. Huang, X. et al. Production of high-purity rutile titanium dioxide by leachingwater-quenched titanium-bearing blast furnace slag withhydrochloric acid. *Iron Steel Vanadium Titanium* **44**, 23–32. https://doi.org/10.7513/j.issn.1004-7638.2023.03.004 (2023).
34. Zhao, L. et al. Influencing factors and mechanism of ultraviolet/chlorine degradation on phenacetin. *Technol. Water Treat.* **45**, 69–73. https://doi.org/10.16796/j.cnki.1000-3770.2019.03.014 (2019).
35. Ministry of Ecology and Environment of the People's Republic of China *Environmental quality standards for surface water*, https://www.mee.gov.cn/ywgz/fgbz/bz/bzwb/shjbh/shjzlbz/200206/t20020601_66497.shtml (2002).
36. Qing, Z. et al. Simply synthesized sodium alginate/zirconium hydrogel as adsorbent for phosphate adsorption from aqueous solution: Performance and mechanisms. *Chemosphere* **291**, 133103. https://doi.org/10.1016/j.chemosphere.2021.133103 (2022).
37. Hu, F. et al. High-efficient adsorption of phosphates from water by hierarchical CuAl/biomass carbon fiber layered double hydroxide. *Colloids Surf. A Physicochem. Eng. Aspects* **555**, 314–323. https://doi.org/10.1016/j.colsurfa.2018.07.010 (2018).
38. Fu, C., Zhu, X., Dong, X., Zhao, P. & Wang, Z. Study of adsorption property and mechanism of lead (II) and cadmium (II) onto sulfhydryl modified attapulgite. *Arab. J. Chem.* **14**, 102960. https://doi.org/10.1016/j.arabjc.2020.102960 (2021).

39. Wang, B. et al. Efficient phosphate elimination from aqueous media by La/Fe bimetallic modified bentonite: Adsorption behavior and inner mechanism. *Chemosphere* **312**, 11. https://doi.org/10.1016/j.chemosphere.2022.137149 (2023).
40. Wang, Y. et al. La (OH) 3 loaded magnetic nanocomposites derived from sugarcane bagasse cellulose for phosphate adsorption: Characterization, performance and mechanism. *Colloids Surf. A: Physicochem. Eng. Aspects* **626**, 127060. https://doi.org/10.1016/j.colsurfa.2021.127060 (2021).
41. Wang, X. *Study on The Catalytic Ozonation of Methylene Blue with Activated Carbon Functionalized by Fe-Mn Binary Oxides* (Harbin Institute of Technology, 2021). https://doi.org/10.27061/d.cnki.ghgdu.2021.002898.
42. Zhang, J. Z., Fischer, C. J. & Ortner, P. B. Potential availability of sedimentary phosphorus to sediment resuspension in Florida Bay. *Glob. Biogeochem. Cycles* https://doi.org/10.1029/2004GB002255 (2004).
43. Zhang, J.-Z. & Huang, X.-L. Effect of temperature and salinity on phosphate sorption on marine sediments. *Environ. Sci. Technol.* **45**, 6831–6837 (2011).
44. Chen, Z. et al. Enhanced adsorption of phosphate on orange peel-based biochar activated by Ca/Zn composite: Adsorption efficiency and mechanisms. *Colloids Surf. A Physicochem. Eng. Aspects* **651**, 129728. https://doi.org/10.1016/j.colsurfa.2022.129728 (2022).
45. Mitrogiannis, D. et al. Removal of phosphate from aqueous solutions by adsorption onto $Ca(OH)_2$ treated natural clinoptilolite. *Chem. Eng. J.* **320**, 510–522. https://doi.org/10.1016/j.cej.2017.03.063 (2017).
46. Qiu, S. et al. Adsorption performance and mechanism of Ca–Al-LDHs prepared by oyster shell and pop can for phosphate from aqueous solutions. *J. Environ. Manag.* **303**, 114235. https://doi.org/10.1016/j.jenvman.2021.114235 (2022).
47. Yuan, M. et al. Enhancing phosphate removal performance in water using La–Ca/Fe–LDH: La loading alleviates ineffective stacking of laminates and increases the number of active adsorption sites. *J. Clean. Prod.* **388**, 135857. https://doi.org/10.1016/j.jclepro.2023.135857 (2023).
48. Wang, M., Zhao, L. & Hou, H. Preparation and characterization of sulfhydryl modified palygoskite and their application for adsorption cadmium. *Res. Environ. Sci.* https://doi.org/10.13198/j.issn.1001-6929.2023.02.11 (2023).
49. Lian, W. et al. Adsorption and photocatalytic degradation of Congo red by δ-FeOOH. *Chin. J. Anal. Lab.* https://doi.org/10.13595/j.cnki.issn1000-0720.2022.070501 (2013).
50. Xia, Z., Fen, S., Li, L., Chen, H. & Huang, W. The preparation of porous calcium phosphate and the study of sugar juice cleaning process. *Food Ind.* **38**, 22–27 (2017).
51. Liu, C., Hu, W., Li, J., Jiang, C. & Chen, W. Preparation of the hydroxyapatite to remove fluorine from groundwater and its removal performance. *China Environ. Sci.* **34**, 58–64. https://doi.org/10.3969/j.issn.1000-6923.2014.01.010 (2014).

Acknowledgements

This work was supported by the National Natural Science Foundation of China (grant number 51864021), and the authors are grateful for the helpful suggestions and evaluations given by many anonymous reviewers.

Author contributions

Y.L: formal analysis, investigation, validation, writing—original draft. Y.C.: conceptualization, formal analysis, investigation, funding acquisition, writing—review and editing. J.X. and J.L.: formal analysis, investigation, methodology, resources.

Competing interests

The authors declare no competing interests.

Ethical approval

This work has not been published before and not under consideration for publication anywhere else.

Additional information

Supplementary Information The online version contains supplementary material available at https://doi.org/10.1038/s41598-024-71347-w.

Correspondence and requests for materials should be addressed to Y.C.